Predictions of the SARS-CoV-2 Omicron Variant (B.1.1.529) Spike Protein Receptor-Binding Domain Structure and Neutralizing Antibody Interactions

Colby T. Ford[1, 2, ✉], **Denis Jacob Machado**[1], **and Daniel A. Janies**[1]

[1]Department of Bioinformatics and Genomics, University of North Carolina at Charlotte, Charlotte, NC, USA
[2]School of Data Science, University of North Carolina at Charlotte, Charlotte, NC USA

The genome of the SARS-CoV-2 Omicron variant (B.1.1.529) was released on November 22, 2021, which has caused a flurry of media attention due the large number of mutations it contains. These raw data have spurred questions around vaccine efficacy. Given that neither the structural information nor the experimentally-derived antibody interaction of this variant are available, we have turned to predictive computational methods to model the mutated structure of the spike protein's receptor binding domain and posit potential changes to vaccine efficacy. In this study, we predict some structural changes in the receptor-binding domain that may reduce antibody interaction, but no drastic changes that would completely evade existing neutralizing antibodies (and therefore current vaccines).

SARS-CoV-2 | COVID-19 | Protein Structure Analysis | Antibodies Bioinformatics | Computational Biology | Machine Learning

Correspondence: ***colby.ford@uncc.edu***

Introduction

A team of researchers from the Botswana-Harvard HIV Reference Laboratory submitted a new SARS-CoV-2 genome sequence to GISAID on November 22, 2021 (GISAID accession. EPI_ISL_6752027). The specimen was taken from a living 59-year-old male from Gaborone, Botswana using a nasopharyngeal swab and was sequenced using a Nanopore MinION device.

This sample's genome contains 60 mutations from the Wuhan-derived reference genome (GenBank accession no. NC_045512.2) (1), 37 of which are in the Spike (S) protein. This variant was given the identifier B.1.1.529 by PANGO lineages (2). On November 26, 2021, the WHO has designated B.1.1.529 as a Variant of Concern (VOC), named Omicron (3).

The emergence of new SARS-CoV-2 variants is expected. Therefore, scientists have advocated for close international monitoring to determine the need for vaccination boosters and redesign (4). Hence, the identification of the omicron variant is not surprising. What is surprising is the number of mutations that the omicron variant accumulated compared to the first sequenced genome of SARS-CoV-2.

Different authors have warned that limited SARS-CoV-2 sampling and sequencing from positive cases, especially from asymptomatic and symptomatic cases that did not require hospitalization, would make it challenging to identify new mutations in the virus. For example, Brito et al. (5) analyzed the spatiotemporal heterogeneity in each country's

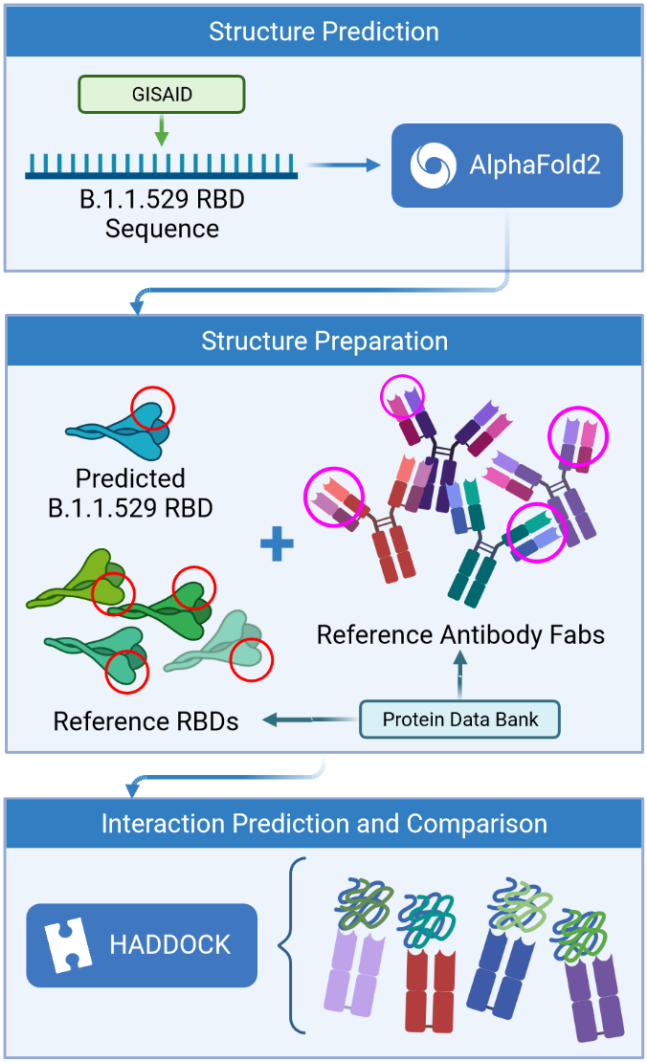

Fig. 1. Process flow of the prediction analysis steps.

SARS-CoV-2 genomic surveillance efforts using metadata submitted to GISAID until May 30, 2021. These authors calculate that sequencing capacity should be at least 0.5% of cases per week when incidence is more than 100 positive cases every 100,000 people. This explains, for example, why Denmark observes greater lineage diversity than most other countries. Brito et al. (5) point out that Denmark's turnaround for sequencing, processing, and sharing SARS-CoV-2 genomic data was less than 18 days, and its sequencing rate

was greater than 32% of cases.

While sampling bias can explain why we may miss new mutations and fail to identify new variants of low prevalence, the emergence of new variants is due to factors that favor the transmission of SARS-CoV-2, including low vaccination rates in some regions, especially in low and middle-income countries (LMICs). Therefore, disparities in vaccination rates combined with sampling bias explain why scientists may continue to be surprised by the mutations in new SARS-CoV-2 variants.

There are many questions regarding genomic epidemiology and the lessons we can learn from the COVID-19 pandemic. Those questions are beyond the scope of this manuscript, and we addressed them elsewhere (6). While the origin and evolution of the Omicron variant are still open questions, here we focus on the potential implications of the mutations observed in this variant.

This seemingly hyper-mutated variant is of public health concern with unanswered questions surrounding vaccine protection (from available vaccines), the possibility of reinfection, transmissibility, and pathogenicity.

Regarding vaccine efficacy, we must look at the receptor-binding domain (RBD), part of the S1 subunit, of the spike protein as this is the binding site for neutralizing antibodies. This domain exists between positions 391 and 541 of the spike protein. Omicron contains 15 mutations in the RBD, none of which are deletions or insertions.

Given that an experimentally-derived structure of the Omicron spike protein is not yet available, we must derive a predicted structure from its sequence *in silico*. Then, we can use available neutralizing antibody structures to computationally model the interaction between Omicron and the paratopes of the antibodies, thus allowing us to compare potential affinity changes due to the mutations and posit their effects to vaccine efficacy.

Methods

Sequence Comparison among VBMs and VOCs. We downloaded the reference genome of SARS-CoV-2 (Wuhan-Hu-1, NCBI's RefSeq accession no. NC_045512.2) as well as the first 100 complete genome sequences ($\geq$29,000 bp) of each Variant of Concern (VOC) and Variant Being Monitored (VBM). The total number of input sequences was 1,301. We aligned all of these complete genomes using `MAFFT` version 7.475 (7) with the "auto" option and trimmed the alignment to remove the 5'-UTR and 3'-UTR regions. We also removed duplicated sequences or sequences with more than 5% of missing data, leaving us with 1,026 sequences.

We annotated each of the 1,026 remaining sequences using the strategy described in Machado et al. (2021) (8). Once we had all the predicted spike proteins for each of the 1,026 genomes, we aligned those sequences based on their translation with the help of `MAFFT` using the `TranslatorX` pipeline (9). We removed duplicated sequences and sequences with more than 5% of missing data. Finally, we identified the receptor biding motif on that alignment based on sequence similarity with the reference.

We then calculated the pairwise p-distances between each pair of sequences were calculated using `MEGA` version 11.0.10 (10). This distance is the proportion (p) of nucleotide sites at which two sequences being compared are different. The p-distances were calculated for the whole spike alignments (nucleotides) but also for the alignment of its receptor binding motif (RBM; position 430–522 of the spike amino acid sequence, a subset of the positions in the RBD).

This variant nucleotide sequence for the spike protein was then translated into amino acids using the standard translation table. This sequence was then trimmed to only contain the RBD of the spike protein (positions 319 to 541).

Receptor-Binding Domain Structural Prediction. Using the derived RBD amino acid sequence for Omicron, we used `AlphaFold2` to create a predicted 3D structure. `AlphaFold2` is a neural network-based deep learning model created by Google DeepMind (11). The algorithm first searches for homologous sequences with existing structures to use as a scaffold on which to place the new sequence.

This prediction was run on the with the "single sequence" mode of `AlphaFold2` using the predicted TM-score (PTM) method. We also specified that the algorithm should run an Amber relaxation procedure to repair any structural violations in the predicted model (12). This resulted in a .PDB file of the predicted RBD structure for Omicron along with metrics surrounding the predicted aligned error (PAE), sequence coverage, and predicted confidence (pLDDT) by position (available in Supplementary Materials).

Neutralizing Antibody Interaction Simulation. Using the predicted structure of the Omicron RBD, we simulated the interaction with four available neutralizing antibody structures: C105, CC12.1, CC12.3, and CV30 (PDBs: 6XCM, 6XC2, 6XC7, and 6XE1, respectively) (13–15). We used only a single fragment antigen-binding (Fab) region of the antibody structures as the paratope location against which to dock. Each of the RBD structures from these reference files have identical sequences to the Wuhan-Hu-1 spike RBD.

Each of these neutralizing antibody structures were collected from patients who had been infected with SARS-CoV-2. All of them bind to the same "up" location of the S1 subunit of the spike protein. This is a similar location to the interaction site between the human ACE2 receptor epitope. Thus, the neutralizing mechanism of these antibodies is in the prevention of SARS-CoV-2 binding to ACE2 on human cells.

We used `HADDOCK` version 2.4, a biomolecular modeling software that provides docking predictions for provided structures, to predict the binding affinity between the epitope of the RBD with the paratope of the neutralizing antibody structures (16). This takes in two or more .PDB files as inputs and outputs multiple predicted protein complexes in .PDB format along with docking metrics.

We first renumbered the residues according to `HADDOCK`'s requirements and then specified the interacting residues between the RBD structure and the Fab. Specifically, ensure there are not overlapping residue IDs between the chains of a .PDB file and then specify the residues that are assumed to

interact between the structures. This analysis was performed on the antibody-RBD structure pairs shown in Table 1.

Antibody Fab	Analysis Type	RBD Source
C105 (6XCM, chains N and S)	Reference	6XCM (chain B)
	Prediction	B.1.1.529 (from AlphaFold2)
CC12.1 (6XC2, chains H and L)	Reference	6XC2 (chain A)
	Prediction	B.1.1.529 (from AlphaFold2)
CC12.3 (6XC7, chains C and D)	Reference	6XC7 (chain A)
	Prediction	B.1.1.529 (from AlphaFold2)
CV30 (6XE1, chains H and L)	Reference	6XE1 (chain B)
	Prediction	B.1.1.529 (from AlphaFold2)

Table 1. List of analyses performed, comparing reference and predicted RBD structures in complex with reference Fab structures.

The assessment of these interactions was measured by multiple biophysical factors including Van der Waals energy, electrostatic energy, desolvation energy, and restraints violation energy, which were collectively used to derive a HADDOCK score to quantify changes in protein-protein interaction resulting from mutations in the RBD. Further, interfacing residues between the RBD and Fab structures were determined to by identifying residues that are within a distance of 1.0 Å^2 or less between the chains of the RBD and the Fab using the *InterfaceResidues* functionality in PyMol version 2.4.1 (17).

We then compared the metrics of the actual complexes (i.e., the real RBD structure and the Fab) versus the predicted RBD of Omicron (with the same Fab). This provides a baseline interaction that was then measured against the mutated interaction with each respective Fab.

Results

Variant Sequence Comparison. Although the Omicron RBM (spike amino acid sequence, positions 430–522) can be efficiently categorized by nine characteristic mutations (S:N440K, S:G446S, S:S447N, S:T478K, S:E484A, S:Q493R, S:G496S, S:Q298R, S:N501Y), at least two of them (S:N440K and S:G446S) may be missing from some samples classified as Omicron. Also, some Omicron RBMs contains an additional mutation at S:Y505H.

The Omicron variant is the variant more distantly related to the reference genome (SARS-CoV-2 Wuhan-Hu-1; NCBI's RefSeq accession no. NC_045512.2) in the proportion of shared nucleotides. Also, Omicron is the variant that is more distantly related to Gamma. See Figures 2 and 3.

Mutational Analysis. Comparing the RBD of Omicron to the reference genome, there are 15 mutations, all of which are single amino acid substitutions. Most of the substitutions result in a change in the residue type. (See Table 2.)

Variant	1	2	3	4	5	6	7	8	9	10	11
1. Reference: Wuhan-Hu-1	0.00%										
2. VBM: B.1.617.3	0.19%	0.00%									
3. VBM: Beta	0.20%	0.32%	0.00%								
4. VBM: Epsilon	0.15%	0.23%	0.31%	0.00%							
5. VBM: Eta	0.23%	0.33%	0.33%	0.32%	0.00%						
6. VBM: Gamma	0.33%	0.43%	0.38%	0.41%	0.46%	0.00%					
7. VBM: Iota	0.17%	0.29%	0.27%	0.26%	0.33%	0.43%	0.00%				
8. VBM: Kappa	0.24%	0.20%	0.37%	0.28%	0.39%	0.49%	0.32%	0.00%			
9. VBM: Mu	0.22%	0.26%	0.27%	0.32%	0.33%	0.40%	0.27%	0.33%	0.00%		
10. VBM: Zeta	0.11%	0.22%	0.21%	0.21%	0.23%	0.29%	0.20%	0.27%	0.23%	0.00%	
11. VOC: Delta	0.23%	0.14%	0.39%	0.26%	0.40%	0.50%	0.34%	0.29%	0.33%	0.29%	0.00%
12. VOC: Omicron	0.81%	0.88%	0.90%	0.90%	0.88%	0.98%	0.84%	0.90%	0.79%	0.86%	0.88%

Fig. 2. Distance matrix of the spike gene (using nucleotides) for 9 Variants Being Monitored (VBM) and 2 Variants of Concern (VOC). The distance is the average proportion (*p*) of nucleotide sites at which two sequences being compared are different.

Variant	1	2	3	4	5	6	7	8	9	10	11
1. Reference: Wuhan-Hu-1	0.00%										
2. VBM: B.1.617.3	2.20%	0.00%									
3. VBM: Beta	2.20%	3.33%	0.00%								
4. VBM: Epsilon	1.09%	1.09%	3.33%	0.00%							
5. VBM: Eta	1.25%	2.36%	1.25%	2.36%	0.00%						
6. VBM: Gamma	2.20%	3.33%	0.00%	3.33%	1.25%	0.00%					
7. VBM: Iota	0.82%	2.67%	2.30%	1.92%	1.34%	2.30%	0.00%				
8. VBM: Kappa	2.20%	0.00%	3.33%	1.09%	2.36%	3.33%	2.67%	0.00%			
9. VBM: Mu	2.20%	3.33%	0.00%	3.33%	1.25%	0.00%	2.30%	3.33%	0.00%		
10. VBM: Zeta	1.13%	2.28%	1.21%	2.24%	0.28%	1.21%	1.22%	2.28%	1.21%	0.00%	
11. VOC: Delta	2.12%	2.12%	4.42%	1.02%	3.42%	4.42%	2.97%	2.12%	4.42%	3.30%	0.00%
12. VOC: Omicron	11.09%	12.43%	9.78%	12.43%	11.28%	9.78%	10.76%	12.43%	9.78%	11.09%	11.27%

Fig. 3. Distance matrix of the receptor biding motif (RBM) of spike gene (using amino acids) for 9 Variants Being Monitored (VBM) and 2 Variants of Concern (VOC). The distance is the average proportion (*p*) of nucleotide sites at which two sequences being compared are different.

The resulting RBD structure from AlphaFold2 shows that there is little conformational change from the reference structure. See Figure 4.

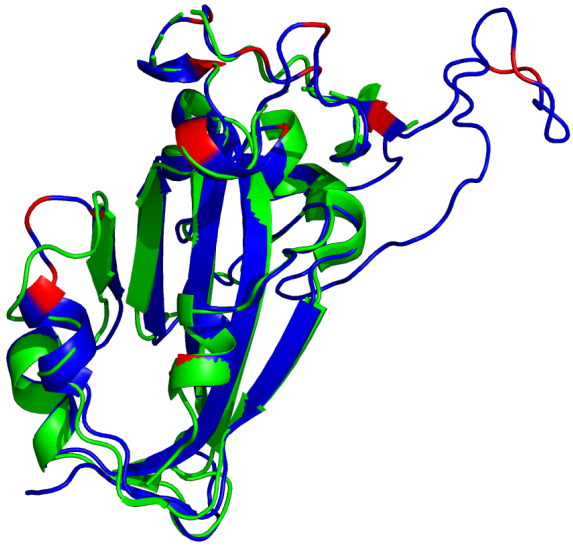

Fig. 4. Comparison of reference RDB structure (PDB: 6XC2, shown in green) and the predicted Omicron (B.1.1.529) RBD structure (shown in blue). Mutated residues are highlighted in red.

However, there are multiple mutated residues (shown in red in Figure 4) in positions that may affect the ability of a neu-

Position	Ref	Alt	Ref Type	Alt Type	Type Difference
339	G	D	Non-Polar	Negative	Yes
371	S	L	Polar	Non-Polar	Yes
373	S	P	Polar	Non-Polar	Yes
375	S	F	Polar	Non-Polar	Yes
417	K	N	Positive	Polar	Yes
440	N	K	Polar	Positive	Yes
446	G	S	Non-Polar	Polar	Yes
477	S	N	Polar	Polar	No
478	T	K	Polar	Positive	Yes
484	E	A	Negative	Non-Polar	Yes
493	Q	R	Polar	Positive	Yes
496	G	S	Non-Polar	Polar	Yes
498	Q	R	Polar	Positive	Yes
501	N	Y	Polar	Polar	No
505	Y	H	Polar	Positive	Yes

Table 2. Mutations in the receptor-binding domain (RBD) of the spike protein in the Omicron variant (B.1.1.529).

tralizing antibody to sufficiently bind. Some of these mutated residues change to much longer side-chained or differently-charged amino acids. For example, there are two "to lysine" mutations: N440K and T478K (i.e., from polar, smaller side chain residues to a positive-charged, longer side chain residue). These types of changes may have an effect on the binding affinity between the RBD and an antibody, either by changing the surface charge on the protein or by inhibiting a tighter antibody interaction.

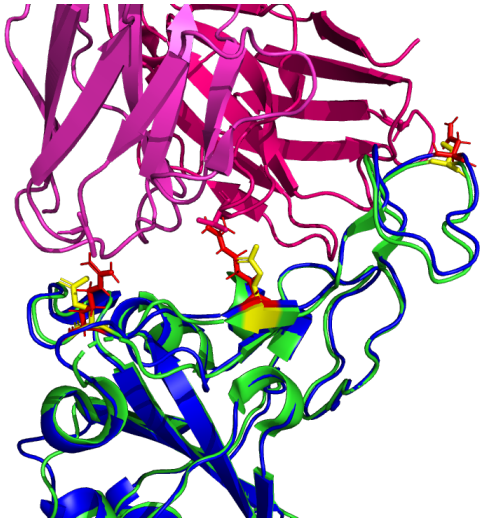

Fig. 5. Possible inhibitory mutated RBD residues in Omicron (B.1.1.529) (structure shown in blue with mutated residues of interest shown in red). Note: the reference RDB structure (PDB: 6XC2 is shown in green with equivalent position residues highlighted in yellow. CC12.1 antibody Fab (from PDB 6XC2) is shown in magenta / pink.

In Figure 5, note how mutations Q498R, N501Y, and S477N from the predicted Omicron (B.1.1.529) structure may affect binding position of the antibody, causing it to bind less effectively. In other words, these longer/larger side chains may increase the distance between the Fab paratope of the antibody and the epitope of the RBD.

Antibody Binding Analyses. The results of all four antibody docking exercises show that the Fab of the respective neutralizing antibodies continue to bind to the RBD of Omicron, though not as well as the reference interaction. Note that there is a consistent decrease (increase in value) in the electrostatic energy and an increase in restraints violation energy between the binding from the reference RBDs and the predicted RBD of Omicron. The HADDOCK score is worse (higher) across the board and it appears that the interaction of the Omicron RBD with the antibodies are more distant, as shown by the buried surface area changes below.

C105 Antibody Binding. Resulting binding metrics from the C105 HADDOCK docking analysis are shown in Table 3. This interaction shows that there is a $\sim 4\%$ reduction in the electrostatic energy and an $\sim 5\%$ decrease in buried surface area comparing between the 6XCM RBD and predicted RBD of Omicron.

Metric	6XCM RBD w/ C105	Predicted B.1.1.529 RBD w/ C105	% Difference
Van der Waals energy	-85.0	-71.8	-16%
Electrostatic energy	-280.9	-268.9	-4%
Desolvation energy	-18.6	-17.1	-8%
Restraints violation energy	154.1	158.8	3%
HADDOCK score	-144.4	-126.8	-12%
Buried Surface Area	2417.8	2299.6	-5%

Table 3. HADDOCK metrics for the CC12.1 docking prediction, comparing the 6XCM RBD vs. the Omicron (B.1.1.529) predicted RDB structure.

Fig. 6. HADDOCK docking prediction using C105 (shown in magenta / pink), comparing the 6XCM RBD (shown in shown in green) vs. the Omicron (B.1.1.529) predicted RDB structure (shown in blue).

CC12.1 Antibody Binding. Resulting binding metrics from the CC12.1 HADDOCK docking analysis are shown in Table 4. This interaction shows that there is a $\sim 17\%$ reduction in the electrostatic energy and an $\sim 7\%$ decrease in buried surface area comparing between the 6XC2 RBD and predicted RBD of Omicron.

Metric	6XC2 RBD w/ CC12.1	Predicted B.1.1.529 RBD w/ CC12.3	% Difference
Van der Waals energy	-106.9	-90.7	-15%
Electrostatic energy	-342.6	-284.9	-17%
Desolvation energy	-37.5	-28.8	-23%
Restraints violation energy	143.2	152.6	7%
HADDOCK score	-198.6	-163.3	-18%
Buried Surface Area	2778.5	2584.3	-7%

Table 4. HADDOCK metrics for the CC12.1 docking prediction, comparing the 6XC2 RBD vs. the Omicron (B.1.1.529) predicted RDB structure.

CC12.3 Antibody Binding. Resulting binding metrics from the CC12.3 HADDOCK docking analysis are shown in Table 4. This interaction shows that there is a $\sim 22\%$ reduction in the electrostatic energy and an $\sim 3\%$ decrease in buried surface area comparing between the 6XC7 RBD and predicted RBD of Omicron.

Metric	6XC7 RBD w/ CC12.3	Predicted B.1.1.529 RBD w/ CC12.3	% Difference
Van der Waals energy	-86.1	-93.1	8%
Electrostatic energy	-248.1	-194.1	-22%
Desolvation energy	-41.7	-37.9	-9%
Restraints violation energy	159.1	104.7	-34%
HADDOCK score	-161.5	-159.4	-1%
Buried Surface Area	2489.8	2416.7	-3%

Table 5. HADDOCK metrics for the CC12.3 docking prediction, comparing the 6XC7 RBD vs. the Omicron (B.1.1.529) predicted RDB structure.

Fig. 7. HADDOCK docking prediction using CC12.1 (shown in magenta / pink), comparing the 6XC2 RBD (shown in shown in green) vs. the Omicron (B.1.1.529) predicted RDB structure (shown in blue).

Fig. 8. HADDOCK docking prediction using CC12.3 (shown in magenta / pink), comparing the 6XC7 RBD (shown in shown in green) vs. the Omicron (B.1.1.529) predicted RDB structure (shown in blue).

CV30 Antibody Binding. Resulting binding metrics from the CV30 HADDOCK docking analysis are shown in Table 6. This interaction shows that there is a $\sim 52\%$ reduction in the electrostatic energy and an $\sim 20\%$ decrease in buried surface area comparing between the 6XE1 RBD and predicted RBD of Omicron.

Metric	6XE1 RBD w/ CV30	Predicted B.1.1.529 RBD w/ CV30	% Difference
Van der Waals energy	-86.1	-61.7	-28%
Electrostatic energy	-354.4	-171.8	-52%
Desolvation energy	-13.8	-19.5	-41%
Restraints violation energy	147.6	159.4	8%
HADDOCK score	-156.0	-99.6	-36%
Buried Surface Area	2479.0	1992.6	-20%

Table 6. HADDOCK metrics for the CV30 docking prediction, comparing the 6XE1 RBD vs. the Omicron (B.1.1.529) predicted RDB structure.

Fig. 9. HADDOCK docking prediction using CV30 (shown in magenta / pink), comparing the 6XE1 RBD (shown in shown in green) vs. the Omicron (B.1.1.529) predicted RDB structure (shown in blue).

Antibody Interaction Comparison. All of the interaction predictions among the four antibodies tested in this study (C105, CC12.1, CC12.3, and CV30) agree that there is a decrease in binding affinity when comparing the respective RBD interactions with the Omicron RBD interaction. We see a drop in electrostatic interaction (increase in the electrostatic energy value) ranging from $\sim 4\%$ to $\sim 52\%$ and a consistent decrease in buried surface area (increase in distance) of the RDB and the antibody Fab. In addition, we see a variable increase (worsening) in the HADDOCK score, indicating that all of the Omicron RBD structures have a lower binding affinity when compared to their respective reference RBD structures as a benchmark. See Figure 10.

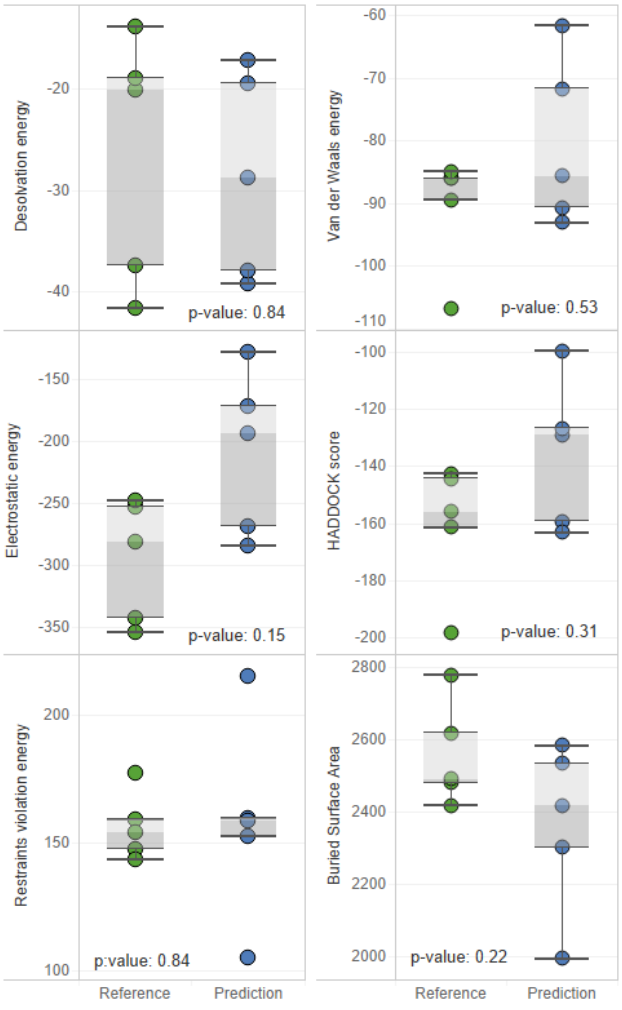

Fig. 10. HADDOCK results comparison between the reference RBD structures and the predicted RBD of Omicron (B.1.1.529). The p-values values corrspond to Wilcoxon Rank-Sum test results.

Interestingly, performing the Wilcoxon Rank-Sum tests on these metrics from Figure 10 to compare the differences between the predictions and reference results shows that there is no statistically-significant difference at the $\alpha = 0.5$ level.

Interface Position		417 (K▶N)	448 (N)	477 (S▶N)	484 (E▶A)	493 (Q▶R)	494 (S)	498 (Q▶R)	501 (N▶Y)	505 (Y▶H)
6XC2 vs. B.1.1.529	*Reference*	K	N	S	E	Q	S	Q	N	Y
	Prediction	N	-	N	-	R	-	R	Y	H
6XC7 vs. B.1.1.529	*Reference*	K	N	S	E	Q	S	Q	N	Y
	Prediction	N	-	N	-	R	-	R	Y	H
6XCM vs. B.1.1.529	*Reference*	K	-	S	E	Q	S	Q	N	Y
	Prediction	N	-	N	-	R	S	R	Y	H
6XE1 vs. B.1.1.529	*Reference*	K	-	S	-	Q	S	Q	N	Y
	Prediction	N	-	-	A	R	S	R	Y	H
Legend: ♦ - Mutated positions with no interface changes, ◯ - Non-mutated positions with interface changes, △ - Mutated positions with interface changes		♦	◯	♦	△	♦	◯	♦	♦	♦

Table 7. Interfacing residue changes of interest between the Fab paratope and the RBD structures. (Note that a '-' means that the residue at this position no longer interfaces with the Fab structure.)

Fab-RBD Interfacing Residues. Furthermore, when comparing residues that are interfaced between the Fab and RBD, there is agreement in that particular residues in Omicron are no longer interfacing with the antibodies analyzed in this study. In particular, residues 448N, 484A, and 494S may not interface with the Fab structure as they are in the reference RBD-Fab complexes. However, the aforementioned N501Y and S477N mutations (along with a variety of other mutations) do not appear to affect the interfacing of the residues at these positions. See Table 7.

This implies that there are certain positions that are more sensitive to mutations in that substitutions at these loci are more likely to affect the interface of the RBD with the antibody's Fab (denoted by a △ symbol in Table 7).

In contrast, there are other positions that have been substituted between the reference RBDs and the predicted Omicron RBD that continue to interface with some or all the Fab structures (denoted by a ♦ symbol in Table 7).

Finally, there are a some residues that remain unchanged in the Omicron variant RBD structure, yet we see changes in the interfacing at these loci (denoted by a ◦ symbol in Table 7). This suggests that there are other mutated residues around these stable positions that may be affecting their ability to interface.

Conclusion and Discussion

While *in vitro* experiments are needed to validate these predictions, the predicted results here suggest that existing neutralizing antibodies will still bind to the mutated spike protein of the Omicron variant. However, it appears that the affinity of Omicrons's RBD for neutralizing antibodies is reduced compared to the reference RBD structures. This result suggests that antibodies elicited from vaccines or a previous infection will provide some protection against Omicron.

Though there are a multitude of mutations in the RBD of Omicron, these mutations do not appear to be causing any large conformational change that would totally evade antibody interaction. However, we do see some amino acid substitutions to different, longer side chained residues at the binding site. This result may be due to the slightly more distant interaction with the antibody and therefore may reduce the binding affinity.

Determining the actual structure of a protein is a time-consuming process. Further, quantifying protein-protein interactions (like spike-to-antibody interactions) are also experimentally difficult to perform *in vitro*. Given the public health urgency in understanding the impacts of new SARS-CoV-2 variants quickly requires that we act quicker than is possible in a lab. Thus, *in silico* predictive tools like `AlphaFold2` and `HADDOCK` are important for quickly understanding the biochemistry of variants and can help us to infer the epidemiological implications of the variant.

Supplementary Materials

All data, scripts, and results from this work are available at GitHub.com/colbyford/SARS-CoV-2_B.1.1.529_Spike-RBD_Predictions (18).

ACKNOWLEDGEMENTS

We acknowledge these entities at UNC Charlotte: The Department of Bioinformatics and Genomics, The Bioinformatics Research Center, the College of Computing and Informatics, The College of Liberal Arts and Sciences, Research and Economic Development, University Research Computing, and the Graduate School. We also thank the Belk family for support.

Bibliography

1. F. Wu, S. Zhao, B. Yu, Y.-M. Chen, W. Wang, Z.-G. Song, Y. Hu, Z.-W. Tao, J.-H.a Tian, Y.-Y.n Pei, M.-L. Yuan, Y.-L. Zhang, F.-H. Dai, Y. Liu, Q.-M.n Wang, J.-J.o Zheng, L. Xu, E. C. Holmes, and Y.-Z. Zhang. A new coronavirus associated with human respiratory disease in China. *Nature*, 579(7798):265–269, 2020. doi: 10.1038/s41586-020-2008-3.
2. A. Rambaut, E. C. Holmes, Á. O'Toole, V. Hill, J. T. McCrone, C. Ruis, L. du Plessis, and O. G. Pybus. A dynamic nomenclature proposal for SARS-CoV-2 lineages to assist genomic epidemiology. *Nature Microbiology*, 5:1403–1407, 2020. doi: 10.1038/s41564-020-0770-5.
3. World Health Organization. *Classification of Omicron (B.1.1.529): SARS-CoV-2 Variant of Concern*, 2021. Available at: https://www.who.int/news/item/26-11-2021-classification-of-omicron-%28b.1.1.529%29-sars-cov-2-variant-of-concern (accessed 1 December 2021).
4. T. Farooqi, J. A. Malik, A. H. Mulla, T. Al Hagbani, K. Almansour, M. A. Ubaid, S. Alghamdi, and S. Anwar. An overview of SARS-CoV-2 epidemiology, mutant variants, vaccines, and management strategies. *Journal of Infection and Public Health*, 14:1299–1312, 2021. doi: 10.1016/j.jiph.2021.08.014.
5. A. F. Brito, E. Semenova, G. Dudas, G. W. Hassler, C. C. Kalinich, M. U.G. Kraemer, S. C. Hill, Danish COVID-19 Genome Consortium, E. C. Sabino, O. G. Pybus, C. Dye, S. Bhatt, S. Flaxamn, M. A. Suchard, N.n D. Grubaugh, G. Baele, and N. R. Faria. Global disparities in SARS-CoV-2 genomic surveillance. *medRxiv*, 2021. doi: 10.1101/2021.08.21.21262393.
6. D. J. Machado, R. A. White III, J. Kofsky, and D. A. Janies. Fundamentals of genomic epidemiology, lessons learned from the coronavirus disease 2019 (covid-19) pandemic, and new directions. *Antimicrobial Stewardship & Healthcare Epidemiology (2021)*, pages 1–11, 2021. doi: 10.1017/ash.2021.222.
7. K. Katoh and Daron M. Standley. Mafft multiple sequence alignment software version 7: improvements in performance and usability. *Molecular biology and evolution*, 30(4):772–780, Apr 2013. ISSN 1537-1719. doi: 10.1093/molbev/mst010. 23329690[pmid].
8. D. Jacob Machado, R. Scott, S. Guirales, and D. A. Janies. Fundamental evolution of all orthocoronavirinae including three deadly lineages descendent from chiroptera-hosted coronaviruses: Sars-cov, mers-cov and sars-cov-2. *Cladistics*, 37(5):461–488, 2021. doi: https://doi.org/10.1111/cla.12454.
9. F. Abascal, R. Zardoya, and M. J. Telford. TranslatorX: multiple alignment of nucleotide sequences guided by amino acid translations. *Nucleic Acids Research*, 38(suppl_2):W7–W13, 04 2010. ISSN 0305-1048. doi: 10.1093/nar/gkq291.
10. G. Stecher, K. Tamura, and S. Kumar. Molecular Evolutionary Genetics Analysis (MEGA) for macOS. *Molecular Biology and Evolution*, 37(4):1237–1239, 01 2020. ISSN 0737-4038. doi: 10.1093/molbev/msz312.
11. J. Jumper, R. Evans, A. Pritzel, T. Green, M. Figurnov, O. Ronneberger, K. Tunyasuvunakool, R. Bates, A. Žídek, A. Potapenko, A. Bridgland, C. Meyer, S. A. A. Kohl, A. J. Ballard, A. Cowie, B. Romera-Paredes, S. Nikolov, R. Jain, J. Adler, T. Back, S. Petersen, D. Reiman, E. Clancy, M. Zielinski, M. Steinegger, M. Pacholska, T. Berghammer, S. Bodenstein, D. Silver, O. Vinyals, A. W. Senior, K. Kavukcuoglu, P. Kohli, and D. Hassabis. Highly accurate protein structure prediction with AlphaFold. *Nature*, 596(7873):583–589, 2021. ISSN 1476-4687. doi: 10.1038/s41586-021-03819-2.
12. V. Hornak, R. Abel, A. Okur, B. Strockbine, A. Roitberg, and C. Simmerling. Comparison of multiple amber force fields and development of improved protein backbone parameters. *Proteins: Structure, Function, and Bioinformatics*, 65(3):712–725, 2006. doi: 10.1002/prot.21123.
13. C. O. Barnes, A. P. West Jr., K. E. Huey-Tubman, M. A.G. Hoffmann, N. G. Sharaf, P. R. Hoffman, N. Koranda, H. B. Gristick, C. Gaebler, F. Muecksch, J. C. C. Lorenzi, S. Finkin, T. Hägglöf, A. Hurley, K. G. Millard, Y. Weisblum, F. Schmidt, T. Hatziioannou, P. D. Bieniasz, M. Caskey, D. F. Robbiani, M. C. Nussenzweig, and P. J. Bjorkman. Structures of human antibodies bound to SARS-CoV-2 spike reveal common epitopes and recurrent features of antibodies. *Cell*, 182(4):828–842.e16, 2020. doi: 10.1016/j.cell.2020.06.025.
14. M. Yuan, H. Liu, N. C. Wu, C.-C. D. Lee, X. Zhu, F. Zhao, D. Huang, W. Yu, Y. Hua, H. Tien, T. F. Rogers, E. Landais, D. Sok, J. G. Jardine, D. R. Burton, and I. A. Wilson. Structural basis of a shared antibody response to SARS-CoV-2. *Science*, 369(6507):1119–1123, 2020. doi: 10.1126/science.abd2321.
15. N. K. Hurlburt, E. Seydoux, Y.-H. Wan, V. V. Edara, A. B. Stuart, J. Feng, M. S. Suthar, A. T. McGuire, L. Stamatatos, and M. Pancera. Structural basis for potent neutralization of SARS-CoV-2 and role of antibody affinity maturation. *Nature Communications*, 11(1):5413, 2020. doi: 10.1038/s41467-020-19231-9.
16. G.C.P. van Zundert, J.P.G.L.M. Rodrigues, M. Trellet, C. Schmitz, P.L. Kastritis, E. Karaca, A.S.J. Melquiond, M. van Dijk, S.J. de Vries, and A.M.J.J. Bonvin. The HADDOCK2.2 web server: User-friendly integrative modeling of biomolecular complexes. *Journal of Molecular Biology*, 428(4):720–725, 2016. doi: 10.1016/j.jmb.2015.09.014.
17. Schrödinger, L. L. C. *The PyMOL Molecular Graphics System, version 2.4.1*, 2015. Available at: http://www.pymol.org/pymol (accessed 29 November 2021).
18. C. T. Ford. *Predictions of the SARS-CoV-2 B.1.1.529 Variant Spike Protein Receptor Binding Domain Structure and Neutralizing Antibody Interactions*, 2021. Available at: https://zenodo.org/record/5733161#.YalzFvFKhhE (accessed 1 December 2021).